

Original Article

Novel composite nano-frameworks for prostate cancer therapy *via* synergistic targeting of ribonucleotide reductase

Mingwei Xu[†], Jun Chen[†], Chengran Huang[†], Cheng Liu^{*}

Department of Urology, Xiangyang Central Hospital, Affiliated Hospital of Hubei University of Arts and Science, 136 Jingzhou Street, Xiangyang, Hubei 441021, P.R.

ARTICLE INFO

Keywords:

Chemodynamic therapy
Deferasirox
Drug resistance
Enzalutamide
Prostate cancer

ABSTRACT

Prostate cancer, a common malignancy in men, poses significant clinical challenges, especially as it progresses to castration-resistant prostate cancer (CRPC). Conventional therapies become less effective due to acquired drug resistance, and even enzalutamide (ENZR), a cornerstone treatment for CRPC, eventually faces resistance. Understanding the clinical significance of ENZR resistance is crucial for improving prostate cancer treatment. To address this issue, we developed an innovative nanosystem: Deferasirox (DEF)-loaded self-etched platinum-cobalt nanodendrites encapsulated within a nanoframe (Pt/Co-ND@DEF). This system combines chemodynamic therapy (CDT) with DEF delivery. Pt/Co-ND@DEF demonstrates potent peroxidase-like activity, catalyzing hydrogen peroxide (H₂O₂) decomposition and glutathione (GSH) depletion to generate reactive oxygen species (ROS). Additionally, DEF release reduces tumor iron ion (Fe³⁺) content, disrupting ribonucleotide reductase activity essential for DNA synthesis and arresting the cell cycle. This dual-action mechanism enhances ROS-induced cytotoxicity and boosts ENZR's efficacy against CRPC, offering a promising multi-target strategy. Our study represents a significant step forward in overcoming ENZR resistance and enhancing prostate cancer treatment, providing new therapeutic avenues for advanced cases.

1. Introduction

Emerging as a pivotal concern within today's healthcare landscape, the increasing prevalence of prostate cancer poses significant challenges. Data from 2020 reveals that prostate cancer stands as the second most common malignancy among men and is the fifth leading cause of cancer-related deaths in males, underscoring its significant public health burden [1,2]. The emergence of CRPC poses significant challenges to conventional androgen deprivation therapy [3]. A distinctive feature of CRPC is the persistence of androgen receptor (AR)-mediated signaling pathways, even at minimal androgen levels [4], consider "prompting the need for innovative treatment approaches.

Enzalutamide (ENZR), an advanced anti-androgen agent, has garnered attention for its superior AR binding affinity, efficiently blocking androgen activity in prostate cancer cells, thus arresting cell cycle progression and tumor growth [5,6]. ENZR has not only secured Food And Drug Administration (FDA) approval for both metastatic and non-metastatic CRPC but also represents a substantial advancement in prostate cancer treatment, surpassing earlier drugs like flutamide and bicalutamide [7,8]. Despite its clinical success, the eventual development of resistance remains a harsh reality for many patients, highlighting the need to understand and overcome this clinical hurdle. In recent years, chemodynamic therapy (CDT) has emerged as a promising therapeutic approach that leverages the Fenton reaction to generate highly cytotoxic hydroxyl radicals in tumor microenvironments, selectively destroying cancer cells [9]. In our

innovative research, we have developed a distinctive nanotechnology solution by integrating CDT with iron chelation drug delivery. This novel approach not only enhances the efficacy of CDT but also ensures targeted drug release, thereby minimizing systemic toxicity and improving treatment outcomes. This breakthrough involves the creation of a Deferasirox (DEF)-embedded self-etching platinum-cobalt nano dendritic framework (Pt/Co-ND@DEF). This novel nanostructure not only exhibits exceptional chemodynamic performance and peroxidase (POD)-like catalytic activity but also possesses superior tumor-targeting capabilities and efficient protein-drug carrier functions, thanks to its unique mesoporous design.

Specifically, Pt/Co-ND@DEF catalyzes the conversion of endogenous hydrogen peroxide (H₂O₂) into hydroxyl radicals (:OH), inducing high levels of oxidative stress while depleting glutathione (GSH). Concurrently, DEF effectively binds intracellular iron ions, forming stable chelates that reduce Fe³⁺ levels, disrupt ribonucleotide reductase activity, and impede cell cycle progression necessary for DNA synthesis [10-12]. This dual mechanism amplifies reactive oxygen species (ROS)-induced cytotoxicity and enhances ENZR's efficacy against CRPC, proposing a multi-target intervention approach (Scheme 1).

Our research unveils new avenues for specifically enhancing the therapeutic potential of prostate cancer treatment by targeting iron metabolism, paving the way for precision oncology. This study could redefine the paradigm of prostate cancer treatment by comprehensively addressing ENZR resistance, offering a more durable and effective option. Moreover, our nanosystem not only suggests a synergistic method to

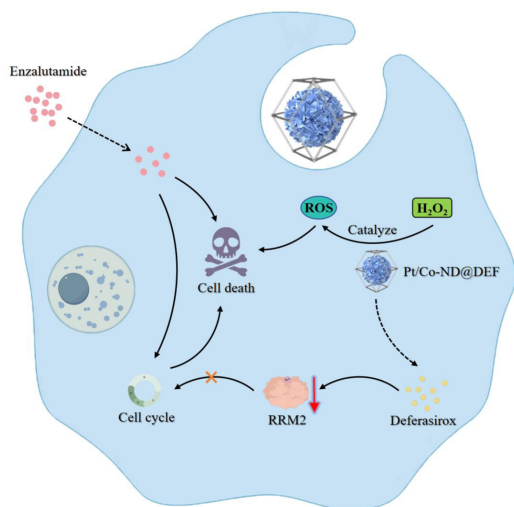
*Corresponding authors:

E-mail addresses: lc19870906@126.com (C. Liu); huangchengran1991@163.com (C. Huang)

[†]Authors contributed equally to this work and shared co-first authorship.

Received: 25 January, 2025 Accepted: 11 February, 2025 Epub Ahead of Print: 07 April 2025 Published: 17 April 2025

DOI: 10.25259/AJC_73_2025



Scheme 1. Schematic illustration of Pt/Co-ND@DEF enhancing the therapeutic effect of ENZR on prostate cancer through synergistic multipathway destruction of the proliferative ability of ENZR-resistant prostate cancer cells.

combat treatment-resistant diseases but also provides clear directions for future research, bringing hope for improved patient outcomes and CRPC management. This study aims to develop and evaluate a novel nanosystem, Pt/Co-ND@DEF that integrates chemodynamic therapy with deferasirox delivery to overcome ENZR resistance and enhance the therapeutic efficacy against CRPC, thereby providing a promising new direction for future clinical treatments.

2. Materials and Methods

2.1. Materials

Hexahydrated hexachloroplatinic acid ($\text{H}_2\text{PtCl}_6 \cdot 6\text{H}_2\text{O}$), cobalt(II) acetylacetonate hydrate [$\text{Co}(\text{acac})_2$, 97% purity], cetyltrimethylammonium bromide (CTAB, 99% purity), oleylamine (OAM, 80-90% purity), and oleic acid (OA, 90% purity) were sourced from Aladdin (Shanghai, China). Experimental water was ultrapure, featuring a resistivity of $18.2 \text{ M}\Omega \cdot \text{cm}$ at 25°C , obtained through a Millipore Milli-Q purification system (Bedford, MA, USA). All chemical reagents, solvents, and materials—including ethanol, methanol, n-hexane, and n-butylamine—were analytical grade and used directly as received.

The cell culture, Roswell Park Memorial Institute (RPMI) 1640 medium, fetal bovine serum (FBS), penicillin-streptomycin mix, 0.25% trypsin-ethylene diamine tetraacetic acid (EDTA) solution, and phosphate-buffered saline (PBS) were procured from Gibco, a division of Thermo Fisher Scientific (Waltham, MA, USA). Culture vessels such as 96-well plates and 10-cm dishes were supplied by Corning Incorporated (NY, USA).

DEF and the Cell Counting Kit-8 (CCK-8) were acquired from Beyotime Biotechnology (Shanghai, China). The assay kit for total glutathione and oxidized glutathione was obtained from the Nanjing Jiancheng Bioengineering Institute (Nanjing, China). Antibodies, including primary and secondary types like rabbit anti-mouse IgG and goat anti-rabbit IgG, were sourced from the Proteintech Group (Wuhan, China).

2.2. Synthesis of Pt/Co-ND and Pt/Co-ND@DEF

To prepare Pt/Co-ND, a Teflon-lined reactor was charged with a mixture including $800 \mu\text{L}$ of distilled water, 62 mg of $\text{Co}(\text{acac})_2$, and 300 mg of CTAB. To this mixture, 8 mL of OAM and 2 mL of OA were added as solvents. The ingredients were then thoroughly combined at ambient temperature through magnetic stirring for 30 mins. Afterward, 0.055 mmol of $\text{H}_2\text{PtCl}_6 \cdot 6\text{H}_2\text{O}$ was incorporated into the blend, followed by continued agitation for another 10 mins to ensure uniform distribution.

The sealed Teflon vessel was placed inside a stainless steel container and submerged in an oil bath set at 180°C . Magnetic

stirring was maintained during the 24-hr reaction period. Once the reaction concluded, the assembly was allowed to cool down to room temperature. The solid product was then isolated using centrifugation at 6000 rpm for 3 mins and purified by successive ethanol washes until all impurities were removed.

In order to fabricate the Pt/Co-ND@DEF complex, 5 mg from the synthesized Pt/Co-ND was mixed with 1 mL of an aqueous DEF solution (concentration: $200 \mu\text{g}/\text{mL}$). This combination was subjected to shaking for 6 hrs to promote conjugation. Following separation from the supernatant via centrifugation and two rounds of ethanol cleansing, the Pt/Co-ND@DEF complex was preserved by lyophilization. The concentration of DEF within the supernatant was quantified using high-performance liquid chromatography (HPLC), employing a Waters e2695 system paired with a 2489 UV detector (produced in the USA), and compared against a standard DEF solution to verify its concentration.

2.3. Characterization

Sophisticated analytical methodologies were employed to thoroughly characterize the nanoparticles, providing an in-depth insight into their attributes. For morphological analysis, a Hitachi SU8220 microscope was utilized for transmission electron microscopy (TEM). Elemental composition mapping was achieved with Thermo Fisher Talos F200X and Talos L 1200C microscopes from Thermo Fisher Scientific, USA. Structural characteristics were elucidated through X-ray diffraction (XRD) data collected on a Bruker D8 Advance diffractometer supplied by Bruker AXS, Germany.

Chemical makeup was scrutinized via X-ray photoelectron spectroscopy (XPS) conducted on a Thermo Scientific K-Alpha spectrometer. Functional group identification was performed using Fourier-transform infrared spectroscopy (FTIR) on a Nicolet 7000-C spectrometer, operating at a resolution of 4 cm^{-1} , with samples prepared as potassium bromide (KBr) discs.

2.4. Stability testing of nanoparticles

To evaluate the stability of the Pt/Co-ND@DEF nanoparticles, a suspension in a 10% FBS-enriched medium was prepared. Changes in the average nanoparticle size and polydispersity index (PDI) were carefully monitored using a particle characterization system for 7 days.

2.5. Establishment of ENZR-resistant C4-2B cell line (C4-2B-ENZR)

The C4-2B cell line, derived from human prostate cancer, was maintained in RPMI-1640 medium supplemented with $100 \text{ IU}/\text{mL}$ penicillin-streptomycin and 10% FBS at a temperature of 37°C . Upon reaching approximately 60% confluence, cells were subjected to treatment with ENZR at a concentration of $5 \mu\text{M}$; control groups received only PBS vehicle. Cells under ENZR exposure were passaged in media containing the same concentration of ENZR, with fresh medium, including the drug being replaced every two days to ensure consistent therapeutic levels.

As the growth rates of treated cells synchronized with those of the control group, the ENZR concentration was incrementally escalated to 10, 20, 30, and finally $40 \mu\text{M}$. After continuous cultivation for four months at the highest concentration, the cells were maintained at this level for an additional six months to assess the development of ENZR resistance. Thereafter, the resistant cell lines were maintained with a reduced ENZR concentration of $20 \mu\text{M}$ for ongoing studies.

2.6. CCK-8 assay

To evaluate the cytotoxic effects of Pt/Co-ND@DEF on C4-2B cells, a CCK-8 assay was employed. Initially, C4-2B cells were plated at a density of 5,000 cells per well in 96-well plates and incubated under conditions of 37°C and 5% CO_2 . Following a 24-hr incubation period to allow cell attachment and stabilization, the culture medium was exchanged for RPMI 1640 medium supplemented with different concentrations of Pt/Co-ND@DEF. The impact on cell viability was then determined through the conventional CCK-8 method. For this purpose, the absorbance of each well was quantified at a wavelength

of 450 nm using a microplate reader, providing a measure of cellular metabolic activity and, by extension, cell health.

2.7. Plate cloning assay

To conduct the cell cloning assay, after digesting and collecting the cells through centrifugation, they were resuspended and their concentration determined. For seeding, each well of a 6-well plate received a mixture of 2 mL culture medium supplemented with serum and an appropriate volume of the cell suspension to achieve approximately 1000 cells per well. This mixture was gently combined and then allowed to incubate until macroscopically discernible colonies developed, a process that typically takes around 10 days.

Upon completion of the incubation period, the medium was carefully removed. Cells were then fixed using a 1 mL application of a 4% paraformaldehyde solution, followed by staining with a 0.1% crystal violet solution; each step lasted for 30 mins. Following fixation and staining, the plates underwent thorough rinsing with water and were left to air dry. Images of the wells were captured, and the quantity of colonies present in each well was quantified.

2.8. Apoptosis detection

Cell apoptosis was evaluated using fluorescein isothiocyanate/propidium iodide (FITC/PI) Annexin V Apoptosis Detection Kits (BD Biosciences). Briefly, 5×10^5 cells were collected, incubated with FITC/PI for 15 mins at room temperature, and then analyzed by flow cytometry (FCM) (Beckman Coulter). For detachment-induced apoptosis, cells were pre-incubated in ultra-low-attachment plates for 24 hrs. C4-2B cells received Pt/Co-ND@DEF or ENZR; double-distilled water served as a negative control.

2.9. Transwell migration assay

To evaluate the migratory capability of cells, we employed 24-well Transwell chambers equipped with 8 μm porous membranes (Corning). Suspensions containing 1×10^5 cells in 200 μL of serum-free medium were placed into the upper compartments, while the lower chambers were filled with complete growth medium. Following a 24-hr incubation period at 37°C, cells that had traversed to the underside of the membrane were fixed using methanol and subsequently stained with a 0.1% crystal violet solution.

The stained cells were then quantified by selecting three arbitrary fields under an inverted phase-contrast microscope (Olympus) set at a magnification of 100x. This method allowed for a thorough assessment of cell migration activity under defined experimental conditions.

2.10. Cell cycle detection

Cells were subjected to digestion, after which they were transferred to centrifuge tubes and subjected to centrifugation for collection. Following this, the cells underwent two wash cycles with PBS, interspersed with an additional centrifugation step; the supernatant was carefully removed following each cycle. To prepare the cells for analysis, 1 mL of a 1 \times DNA staining solution along with 10 μL of permeabilization reagent was added to the cell pellet, ensuring thorough resuspension. The samples were gently mixed via pipetting and subsequently incubated in darkness at room temperature for 30 mins. Finally, FCM was employed to evaluate the prepared samples.

2.11. Western blotting

For the analysis of cellular protein expression, proteins were isolated using the RIPA buffer supplemented with protease inhibitors. Protein concentrations were determined using a bicinchoninic acid (BCA) assay kit supplied by Nanjing Jiancheng Bioengineering. Equal amounts of protein were then subjected to sodium dodecyl sulfate polyacrylamide gel electrophoresis (SDS-PAGE) on polyacrylamide gels.

Following electrophoresis, proteins were transferred onto PVDF membranes. After blocking non-specific binding sites, the membranes were incubated overnight at 4°C with primary antibodies targeting

ribonucleotide reductase (RR) subunit M2 (RRM2), AR, androgen receptor variant 7 (AR-V7), aldo-keto reductase family 1, member C3 (AKR1C3), or glyceraldehyde-3-phosphate dehydrogenase (GAPDH) (all obtained from Proteintech). Subsequently, the membranes were incubated with the appropriate secondary antibodies for two hrs at room temperature. The antibody-bound proteins were detected using an enhanced chemiluminescence (ECL) system, and the resulting bands were quantified using ImageJ software for further analysis.

2.12. Reactive oxygen species (ROS) detection

To determine the intracellular ROS levels in prostate cancer cells, we utilized the Dichlorodihydrofluorescein-diacetate (DCFH-DA) fluorescent probe (provided by Sigma) according to the manufacturer's protocol. After staining the cells with DCFH-DA and counterstaining with 4',6-diamidino-2-phenylindole (DAPI) for nuclear highlighting, fluorescence microscopy was employed to examine the samples. In this analysis, DCFH-DA served as the indicator for ROS detection, whereas DAPI enabled a distinct view of the nuclei. Fluorescence microscopy was subsequently used to evaluate ROS concentrations within the prostate cancer cells, offering valuable insights into ROS accumulation.

2.13. Mitochondrial Membrane Potential (MMP) detection

To evaluate the MMP in prostate cancer cells after treatment with Pt/Co-ND@DEF, we utilized the JC-1 kit supplied by Multisciences, following the manufacturer's instructions. Post-treatment, the cells underwent incubation with the JC-1 dye solution and were then analyzed by FCM on a BD LSRFortessa™ X-20 system.

2.14. Tumor xenografts

Fifteen 4-week-old male Bagg albino c (BALB/c) nude mice were randomly divided into three groups ($n = 5$ per group): Control, Pt/Co-ND@DEF, and Pt/Co-ND@DEF + ENZR. All mice were subcutaneously inoculated with C4-2B-ENZR cells. All procedures involving animals were conducted in accordance with protocols approved by the Animal Care Committee of Hubei University of Arts and Science.

2.15. Statistical analysis

Data were analyzed by GraphPad Prism 7.0 and expressed as mean \pm Standard Error of the Mean. Groups were compared by the Student's t-test. One-way Analysis of variance (ANOVA) evaluated differences between groups. $P < 0.05$ indicated statistical significance.

3. Results and Discussion

3.1. Synthesis and characterization of Pt/Co-ND

As illustrated in Figure 1(a), the transmission electron microscopy (TEM) images unveil the distinctive morphological characteristics of Pt/Co-ND: they exhibit a flower-like nanostructure encased within a framework-type shell, with individual nanoparticles measuring approximately 100 nm in size. To further investigate the composition of Pt/Co-ND, high-angle annular dark-field scanning transmission electron microscopy (HAADF-STEM) was employed in conjunction with energy-dispersive X-ray spectroscopy (EDS) mapping. As shown in Figure 1(b), the acquired images demonstrate an even distribution of platinum (Pt) and cobalt (Co) elements throughout the structure of Pt/Co-ND. The elemental analysis results are detailed in Figure 1(c), which further confirms the presence of these two atomic constituents. X-ray diffraction (XRD) data analysis reveals that the diffraction peaks at angles of 40.3°, 46.9°, and 68.7° corresponding to the (111), (200), and (222) crystal planes of the Pt-Co alloy, respectively (Figure 1d). These planes are also clearly visible in the high-resolution diffraction patterns (Figure 1e).

Additionally, we examined the POD-like activity under simulated acidic conditions using a colorimetric assay. The results indicate a Michaelis-Menten constant (Km) of 0.4627 and a Vmax of 3.5354×10^{-7} M, attesting to its efficient performance under these conditions

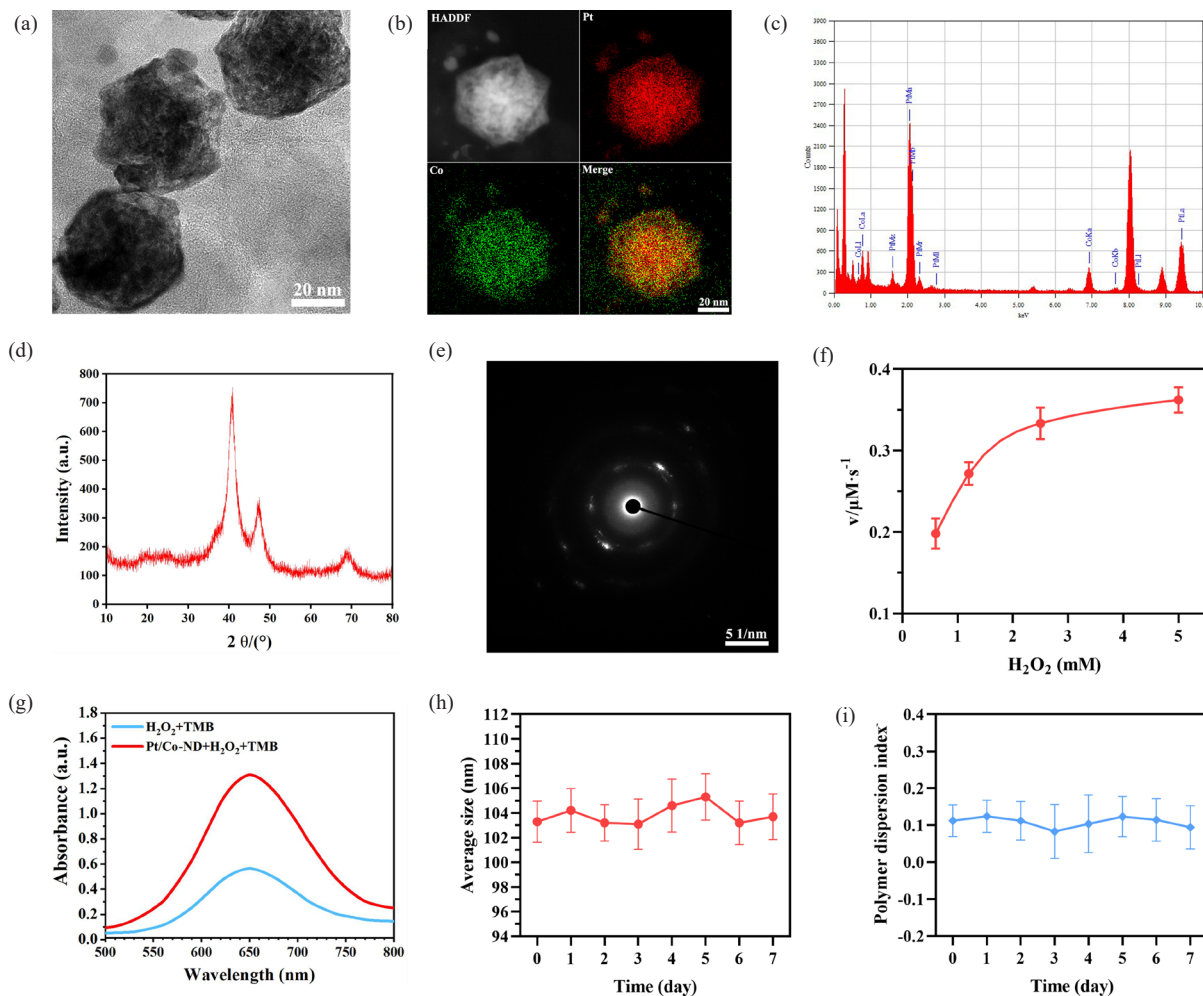


Figure 1. The characterization of Pt/Co-ND. (a) Transmission electron microscopy (TEM) image illustrating the morphology of Pt/Co-ND. (b) High-angle annular dark-field (HAADF) scanning transmission electron microscopy images alongside their associated elemental distribution maps for Pt/Co-ND. (c) Energy-dispersive X-ray spectroscopy (EDS) analysis of Pt/Co-ND, highlighting the characteristic elemental peaks. (d) X-ray diffraction (XRD) profile of Pt/Co-ND, indicating the crystalline structure. (e) Selected-area electron diffraction (SAED) pattern obtained from Pt/Co-ND, revealing its lattice structure. (f) Kinetic study of Pt/Co-ND using Michaelis-Menten analysis with H_2O_2 as the reactant. (g) Ultraviolet-visible (UV-vis) absorbance curves of TMB at an optimal wavelength of 652 nm after reaction. (h) Statistical summary presenting the mean size and (i) polydispersity index (PDI) of Pt/Co-ND following one week of storage under ambient conditions. Pt/Co-ND: Platinum/cobalt nanodots.

(Figure 1f). For further evaluation of the POD-like activity and pro-oxidative stress capabilities of Pt/Co-ND@DEF, we monitored hydroxyl radical generation using 3,3',5,5'-tetramethylbenzidine (TMB) as an indicator. As seen in Figure 1(g), the significant increase in absorbance at 652 nm indicates the outstanding ability of this composite material to induce oxidative stress. These observations not only confirm the exceptional POD-like activity of Pt/Co-ND but also highlight its potential for applications in cancer therapy.

Moreover, Pt/Co-ND displayed consistent hydrodynamic diameter (Dh) and polydispersity index (PDI) over a period of 7 days in media containing 10% FBS, as depicted in Figure 1(h-i), demonstrating good stability under physiological conditions.

3.2. Pt/Co-ND@DEF inhibits prostate cancer cell growth effectively

To comprehensively explore the anticancer potential of Pt/Co-ND@DEF, we conducted a CCK-8 assay to examine how different concentrations (ranging from 0 to 64 $\mu\text{g}/\text{mL}$) of Pt/Co-ND and Pt/Co-ND@DEF affect the proliferation of the C4-2B prostate cancer cell line. Our findings showed that Pt/Co-ND significantly reduced cell proliferation, with Pt/Co-ND@DEF demonstrating a stronger dose-dependent inhibitory effect (Figure 2a). Notably, at 8 $\mu\text{g}/\text{mL}$, Pt/Co-ND@DEF achieved approximately 50% cell mortality, leading us to choose this concentration for further studies.

The therapeutic effectiveness of Pt/Co-ND@DEF against prostate cancer cells was also confirmed using live/dead cell staining with Calcein-AM/PI (Figure 2b). FCM analysis revealed that Pt/Co-ND@DEF markedly increased apoptosis in these cells (Figure 2c-d). Moreover, the clonogenic survival assay demonstrated that Pt/Co-ND@DEF considerably diminished the cells' colony-forming capability (Figure 2e-f).

In conclusion, our results highlight the superior antitumor activity of Pt/Co-ND@DEF against prostate cancer and provide strong evidence supporting its development as a promising anticancer agent.

3.3. Pt/Co-ND@DEF exhibits excellent POD-like activity and inhibits RRM2 expression

To further investigate the potential of Pt/Co-ND in elevating ROS levels in prostate cancer cells, we utilized the DCFH-DA probe [13,14]. As illustrated in Figure 3(a-b), cells exposed to Pt/Co-ND showed a markedly increased fluorescence intensity relative to untreated controls. This finding suggests that Pt/Co-ND exhibits robust POD-like activity, capable of inducing significant oxidative stress within prostate cancer cells. Such heightened oxidative pressure can impair MMP, leading to depolarization of MMP and apoptosis [15,16].

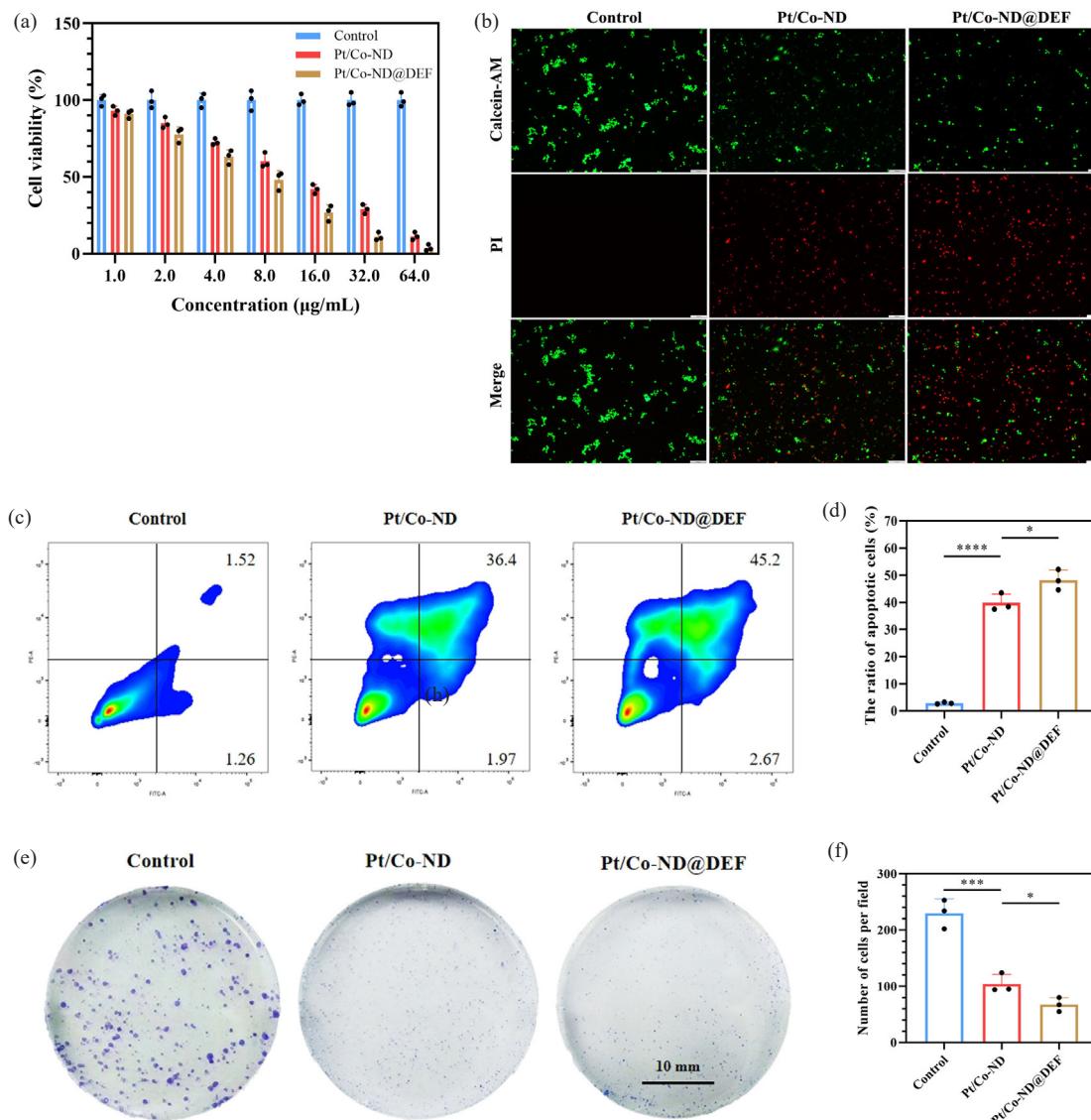


Figure 2. Pt/Co-ND and Pt/Co-ND@DEF induced apoptosis in prostate cancer cells. (a) Cell viability is measured by CCK-8 assay. (b) Fluorescence images of the live/dead cell viability assay kit (Calcein-AM/PI) stained prostate cancer cells (scale bar = 100 µm). (c-d) The apoptosis of prostate cancer cells is analyzed by FCM with staining Annexin-V-APC/PI. (e) Cell growth assessed by colony formation assay in prostate cancer cells (scale bar = 10 mm) and (f) corresponding quantitative analysis (scale bar = 10 mm). * $p < 0.05$; ** $p < 0.01$; *** $p < 0.001$. Pt/Co-ND: Platinum/cobalt nanodots, Pt/Co-ND@DEF: Platinum/cobalt nanodots functionalized with DEF, CCK-8: Cell counting kit-8, Calcein-AM/PI: Calcein-AM/propidium iodide, FCM: Flow cytometry, Annexin-V-APC: Annexin-V allophycocyanin, PI: Propidium iodide.

To explore the impact of Pt/Co-ND on MMP changes in prostate cancer cells systematically, we conducted FCM analysis on JC-1-stained C4-2B cells. Under normal physiological conditions, JC-1 dye selectively accumulates within intact mitochondria, forming aggregates that emit a strong red fluorescence detectable through the FL1 channel. This red fluorescence serves as an indicator of healthy MMP. Conversely, when MMP is compromised or disrupted, JC-1 fails to aggregate and instead exists as monomers that emit green fluorescence, which can be observed via the FL2 channel [17]. The shift from red to green fluorescence thus reflects a reduction in MMP, providing a reliable method for assessing mitochondrial function [15]. Our findings revealed that while both control and treated groups initially exhibited strong red fluorescence with minimal green signals, indicating stable MMP at this point (Figure 3c-d), the Pt/Co-ND treatment group later demonstrated a pronounced increase in green fluorescence. This shift confirms the superior ROS-inducing capability of Pt/Co-ND and its effective role in promoting MMP depolarization and damage (Figure 3c-d).

Moreover, DEF, released from the Pt/Co-ND@DEF complex, is a novel iron chelator suitable for both animal and human use, exhibiting adjuvant anticancer effects. These effects are associated with inhibiting the activity of ribonucleotide reductase (RR) subunit M2 (RRM2)

within tumor cells. RR forms heterodimers composed of M1 and M2 subunits, with M2 expression upregulated during the S phase of the cell cycle [18]. This subunit contains a binuclear iron center and a tyrosyl radical, both critical for RRM2 activity [18]. The maintenance of newly synthesized RRM2 activity requires a stable iron supply [19,20]. DEF effectively chelates iron in tumor tissues, blocking cellular iron uptake thereby suppressing RR activity. Our research found that Pt/Co-ND@DEF markedly reduced RRM2 expression levels in prostate cancer cells (Figure 3e-f). This suggests that Pt/Co-ND@DEF releases DEF, which can efficiently chelate iron within tumor tissues, thus interrupting RRM2 activity and exerting its anticancer function.

3.4. Construction of an ENZR-resistant cell model

ENZR resistance in prostate cancer represents a significant clinical challenge. To delve deeper into the mechanisms underlying this resistance, we successfully developed an ENZR-resistant cell line derived from C4-2B cells, designated as C4-2B-ENZR. In evaluating the sensitivity of these cells to ENZR, our findings revealed that C4-2B-ENZR cells exhibit markedly enhanced survival compared to their parental counterparts. Specifically, after 48-hr treatments with varying

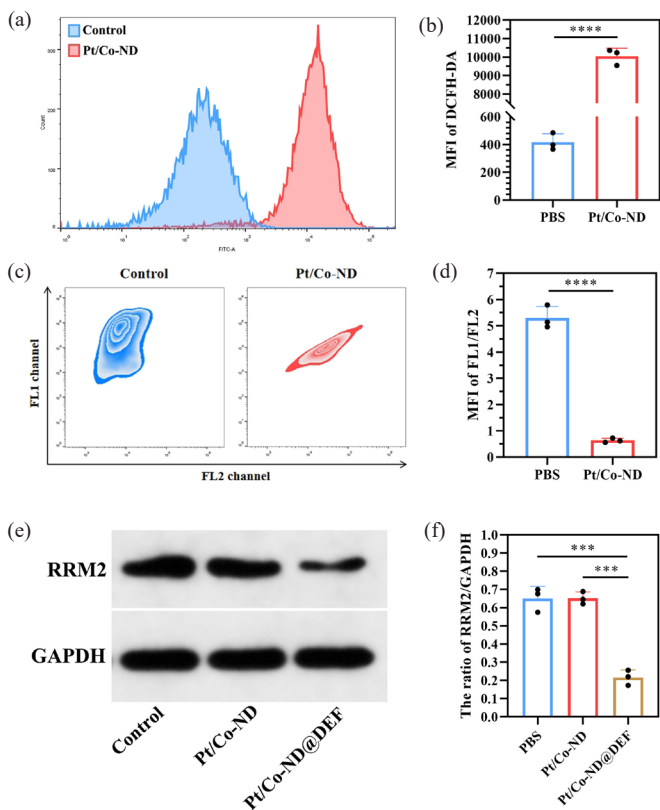


Figure 3. Pt/Co-ND@DEF promoted oxidative stress and inhibits RRM2 activity in prostate cancer cells. (a-b) The ROS levels in prostate cancer cells was detected by DCFH-DA probes. (c-d) The MMP of prostate cancer cells was detected by JC-1 probes. (e-f) The expression of RRM2 was detected by Western Blotting. * $p < 0.05$; ** $p < 0.01$; *** $p < 0.001$. Pt/Co-ND@DEF: Platinum/cobalt nanodots functionalized with DEF, ROS: Reactive oxygen species, DCFH-DA: 2',7'-Dichlorodihydrofluorescein diacetate, MMP: Mitochondrial membrane potential, RRM2: Ribonucleotide reductase M2.

concentrations of ENZR, the half-maximal inhibitory concentration (IC50) values indicated that the IC50 for C4-2B-ENZR cells was 6.4-fold higher than for the parent C4-2B cells (see Figure 4a). Moreover,

within the range of 0 to 320 μM ENZR, the viability of C4-2B-ENZR cells significantly surpassed that of the original cells (see Figure 4b). Notably, at a concentration of 20 μM ENZR, the proliferative capacity of the resistant C4-2B-ENZR cells was notably greater than that of the parental C4-2B cells (Figure 4c).

Our subsequent investigations focused on three proteins—AR, AR-v7, and AKR1C3—that have been established as markers closely associated with ENZ resistance in prostate cancer [21]. Western blot analysis revealed that the expression levels of these three proteins were significantly elevated in C4-2B-ENZR cells relative to those in the parental C4-2B cells (Figure 4d-g). These results suggest that C4-2B-ENZR cells may confer resistance to ENZR through augmented signaling via the AR pathway. Collectively, our findings demonstrate that the C4-2B-ENZR cell line not only possesses resistant characteristics but also serves as a valuable *in vitro* model for investigating the mechanisms of ENZR resistance in prostate cancer.

3.5. Pt/Co-ND@DEF enhanced the sensitivity of C4-2B-ENZR cells to ENZR

We investigated the effects of different concentrations (ranging from 0 to 160 $\mu\text{g}/\text{mL}$) of Pt/Co-ND and Pt/Co-ND@DEF on the proliferative activity of C4-2B-ENZR cells. The data obtained reveal a significant dose-dependent inhibition of cell proliferation by both compounds. Specifically, the IC50 values for Pt/Co-ND and Pt/Co-ND@DEF were determined to be 29.69 $\mu\text{g}/\text{mL}$ and 17.99 $\mu\text{g}/\text{mL}$, respectively, when applied to C4-2B-ENZR cells (Figure 5a). This evidence strongly implies that Pt/Co-ND@DEF may possess potent cytotoxic properties against ENZR-resistant prostate cancer cells, highlighting its potential as a therapeutic agent for further investigation.

We conducted a combination treatment to investigate whether Pt/Co-ND@DEF could enhance the sensitivity of C4-2B-ENZR cells to ENZR. Utilizing methods such as CCK-8 assays, Calcein-AM/PI dual staining, colony formation tests, and FCM, we comprehensively assessed the effects of Pt/Co-ND or Pt/Co-ND@DEF combined with ENZR on cellular proliferation and apoptosis. The results indicated that compared to monotherapy with either agent alone, the combination therapy displayed superior antitumor efficacy. Specifically, Pt/Co-ND@DEF not only possesses inherent anticancer properties but also potentiates the inhibitory effect of ENZR on prostate cancer cells, leading to a marked reduction in cell proliferation, decreased clonogenic capacity, and increased levels of apoptosis (Figure 5b-e).

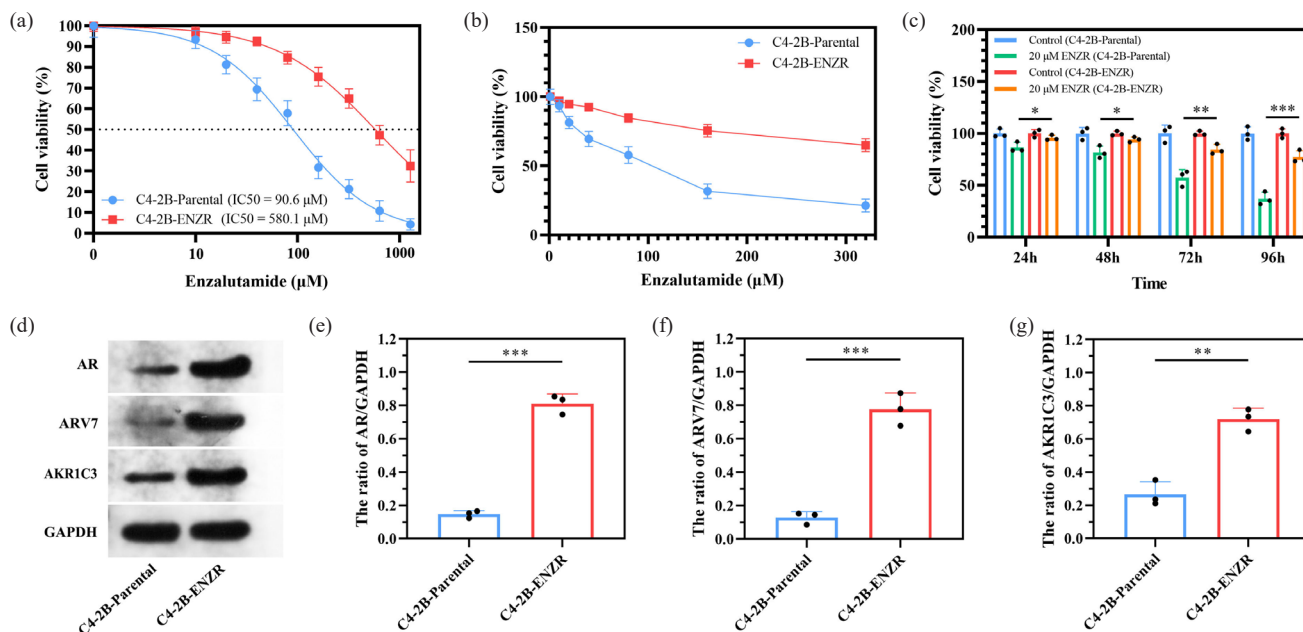


Figure 4. ENZR resistant C4-2B-ENZR cell model is established. (a) IC50 value in C4-2B-ENZR and C4-2B-parental cells. (b) The cell viability is measured by CCK-8 assay in the indicated cell lines under ENZR treatment. (c) Cell growth of C4-2B-parental or C4-2B-ENZR cells treated with 20 μM ENZR. (d-g) The expression of ENZR resistance related molecules were examined by Western Blotting. * $p < 0.05$; ** $p < 0.01$; *** $p < 0.001$. CCK-8: Cell counting kit-8, IC50: 50% inhibitory concentration, ENZR: Enzalutamide resistance.

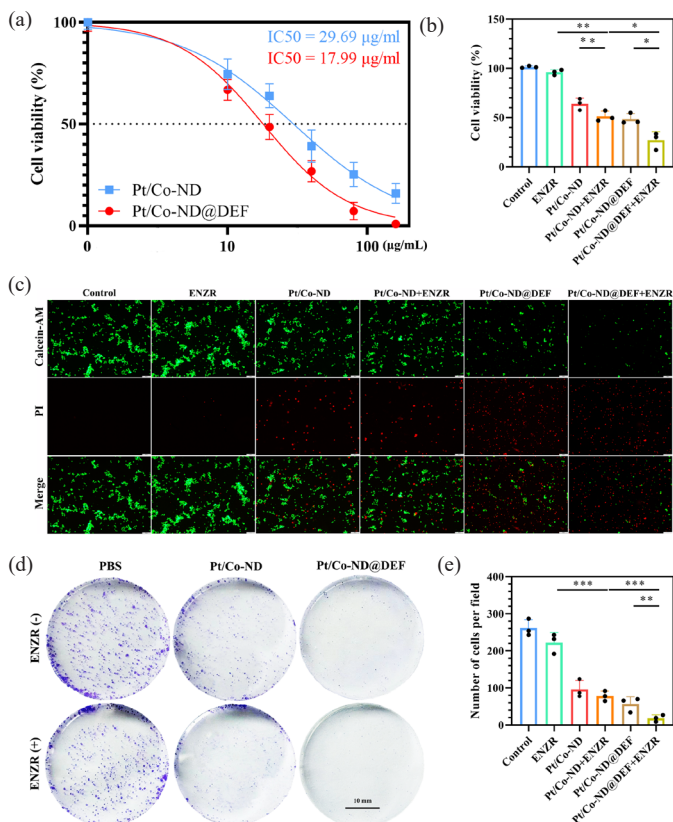


Figure 5. Pt/Co-ND@DEF induced apoptosis in C4-2b-ENZR cells. (a) IC50 value in C4-2b-ENZR cells. (b) Cell viability is measured by CCK-8 assay. (c) Fluorescence images of Calcein-AM/PI stained C4-2b-ENZR cells (scale bar = 100 µm). (d) Cell growth assessed by colony formation assay in prostate cancer cells (scale bar = 10 mm) and (e) corresponding quantitative analysis (scale bar = 10 mm). * $p < 0.05$; ** $p < 0.01$; *** $p < 0.001$.

In conclusion, our study indicates that Pt/Co-ND@DEF can effectively reduce the resistance of prostate cancer cells to ENZR. Moreover, when used in conjunction with ENZR, Pt/Co-ND@DEF demonstrates enhanced anticancer activity against prostate cancer, revealing a significant synergistic effect between the two agents.

3.6. Pt/Co-ND@DEF induces cell cycle arrest and inhibits migration in C4-2B-ENZR cells

Elevated levels of oxidative stress are closely associated with apoptosis, migration, and metastasis in tumor cells [22,23]. The Pt/Co-ND@DEF complex exhibits significant POD-like activity, inducing oxidative stress in prostate cancer cells and effectively inhibiting the function of the RRM2 protein. Increased RRM2 activity is known to be directly linked to the progression and spread of malignant tumors [24]. This protein not only collaborates with multiple oncogenes to facilitate the transformation of normal cells into cancerous ones but also enhances the motility and invasiveness of cancer cells.

In light of these findings, we employed the Transwell assay to evaluate the impact of Pt/Co-ND@DEF on the migratory behavior of C4-2B-ENZR cells. Our results revealed that Pt/Co-ND@DEF significantly restricts the migratory capacity of C4-2B-ENZR cells, with this inhibition being particularly pronounced when used in conjunction with ENZR (Figure 6a-b).

RRM2 plays a crucial role in DNA synthesis and repair by supplying the necessary deoxyribonucleoside triphosphate (dNTPs) precursors and maintaining their pool balance, which is vital for cell proliferation. When RRM2 activity is suppressed, it leads to decreased intracellular dNTP levels, hindering DNA synthesis and repair and causing cell cycle arrest [25]. Additionally, intense oxidative stress can also disrupt the cell cycle of tumor cells. To further explore the effect of Pt/Co-ND@

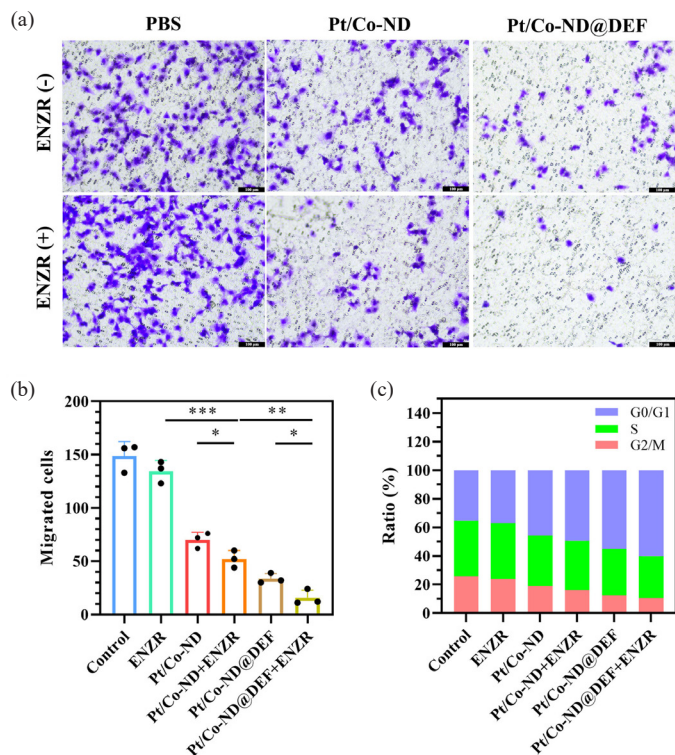


Figure 6. Pt/Co-ND@DEF inhibited the migration and induces cell cycle arrest of C4-2b-ENZR cells. (a) The migration of C4-2b-ENZR cells is measured by Transwell assays. (b) The quantitative analysis of Transwell assays. (c) The cell cycle is analyzed by FCM. * $p < 0.05$; ** $p < 0.01$; *** $p < 0.001$.

DEF on the cell cycle of prostate cancer cells, we conducted relevant studies. According to the data presented in Figure 6(c), both Pt/Co-ND and Pt/Co-ND@DEF induce G0/G1 phase cell cycle arrest in C4-2B-ENZR cells, with Pt/Co-ND@DEF demonstrating a particularly pronounced effect. This suggests that the generation of high levels of ROS by Pt/Co-ND significantly enhances the ability of ENZR to inhibit the cell cycle in prostate cancer cells. In summary, these findings indicate that Pt/Co-ND@DEF not only increases the sensitivity of C4-2B-ENZR cells to ENZR but also effectively suppresses cell migration, resulting in G0/G1 phase cell cycle arrest. Consequently, this leads to effective inhibition of proliferation in prostate cancer cells. This discovery further underscores the potential value of Pt/Co-ND@DEF in the treatment of prostate cancer.

3.7. Anti-cancer effect of Pt/Co-ND@DEF in vivo

We established a cell-derived xenograft (CDX) model based on C4-2B-ENZR cells to evaluate the *in vivo* efficacy of Pt/Co-ND@DEF complexes against prostate cancer (Figure 7a). To monitor tumor progression, tumor volumes were measured every three days post-inoculation. Upon reaching approximately 1 cm³, the experimental animals were euthanized, and tumors were excised and weighed. The images of the tumors revealed that those treated with Pt/Co-ND@DEF were notably smaller compared to the control group. Moreover, in the cohort receiving combined treatment with Pt/Co-ND@DEF and ENZR, tumor sizes were further reduced, with complete regression observed in two mice (Figure 7b-d). These findings indicate that Pt/Co-ND@DEF not only effectively suppresses the growth of xenografts derived from resistant cells but also enhances the sensitivity of C4-2B-ENZR cells to ENZR. The combination of ENZR with Pt/Co-ND@DEF shows considerable promise in combating prostate cancer.

Histological analysis via hematoxylin and eosin (H&E) staining demonstrated more pronounced signs of tumor damage in the group treated with the combination of ENZR and Pt/Co-ND@DEF compared to the control and Pt/Co-ND@DEF alone groups (Figure 7e). Furthermore, terminal deoxynucleotidyl transferase dUTP nick end labeling (TUNEL)

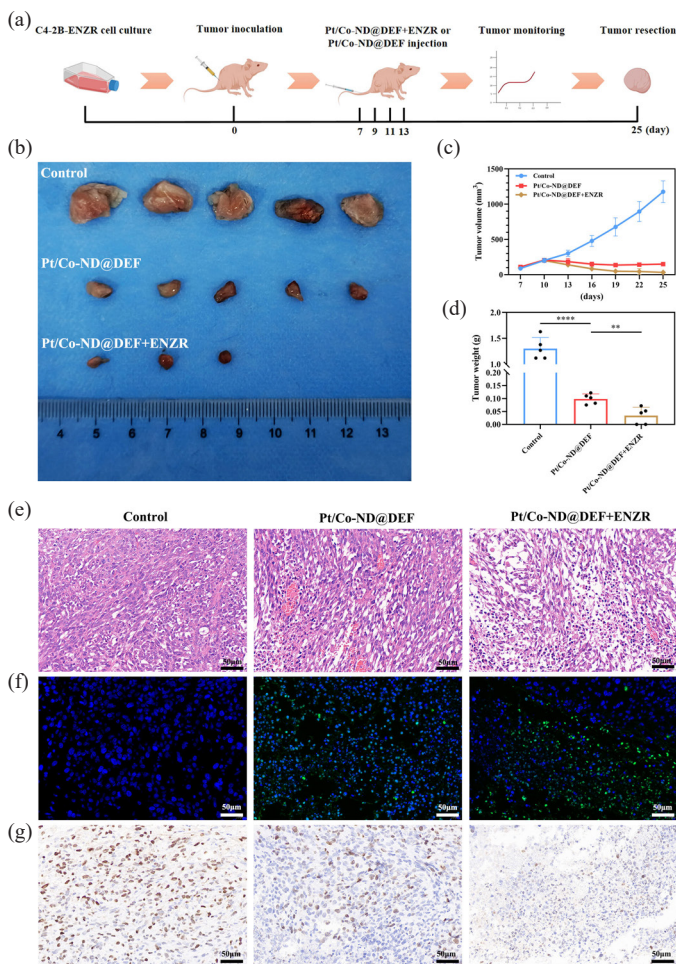


Figure 7. The antitumor effect of Pt/Co-ND@DEF *in vivo*. (a) Schematic illustration of the process of injection of Pt/Co-ND@DEF or Pt/Co-ND@DEF+ENZR in CDX model mice. (b) Digital photographs of tumors in each group. (c) Relative tumor growth curves of C4-2B-ENZR-tumor-bearing mice after tail vein injection of Pt/Co-ND@DEF or Pt/Co-ND@DEF+ENZR and its controls. (d) Tumor weight after 25-days treatment with Pt/Co-ND@DEF or Pt/Co-ND@DEF+ENZR and its controls. (e) Hematoxylin & eosin staining of tumor tissue and its magnified images after treatment by Pt/Co-ND@DEF or Pt/Co-ND@DEF+ENZR and its controls (scale bar = 50 μ m, mag = 200x). (f) TUNEL staining of sections of tumor tissues from mice after treatment by Pt/Co-ND@DEF or Pt/Co-ND@DEF+ENZR and its controls (scale bar = 50 μ m, mag = 200x). (g) Ki67 staining of sections of tumor tissues from mice after treatment by Pt/Co-ND@DEF or Pt/Co-ND@DEF+ENZR and its controls (scale bar = 50 μ m, mag = 200x). * $p < 0.05$; ** $p < 0.01$; *** $p < 0.001$; **** $p < 0.0001$.

assays confirmed an increase in apoptotic cells within the tumor tissue following the combined therapy (Figure 7f), consistent with our observations of apoptosis induction *in vitro*. Ki67 immunohistochemical staining (Figure 7g) similarly evidenced decreased tumor proliferation, marked by a reduction in the number of positively stained cells (brown). Collectively, these results highlight the exceptional *in vivo* antitumor activity of this combinational therapeutic approach.

4. Conclusions

This study focuses on prostate cancer, particularly the formidable challenges encountered in the clinical treatment of prostate cancer, proposing an innovative solution. With the increasing incidence of prostate cancer and the growing resistance of prostate cancer to conventional therapies, exploring effective therapeutic strategies has become a critical issue that modern medicine urgently needs to address. Although ENZR, as a new-generation anti-androgen drug, has demonstrated significant efficacy in inhibiting androgen activity in prostate cancer cells and achieved important clinical milestones, the development of acquired resistance in patients limits its long-term effectiveness.

To tackle this challenge, we have developed a novel nanosystem: self-etching platinum-cobalt nanodendrites nano-frameworks loaded with DEF (Pt/Co-ND@DEF). This system integrates CDT with DEF delivery, offering a new therapeutic avenue. Our research reveals that Pt/Co-ND@DEF exhibits remarkable POD-like activity, capable of catalyzing the decomposition of endogenous H₂O₂ and depleting GSH, thereby generating substantial amounts of ROS. Concurrently, the effective release of DEF reduces the levels of Fe³⁺ within tumors, disrupting ribonucleotide reductase activity—a key factor in DNA synthesis—and thus impeding cell cycle progression. This dual mechanism not only enhances ROS-induced cytotoxicity but also significantly improves the therapeutic effect of ENZR on prostate cancer, demonstrating the potential of complex multi-target intervention strategies.

This research represents a significant advance in overcoming ENZR resistance and enhancing the efficacy of CRPC treatments, paving the way for promising future therapeutic directions. The introduction of the Pt/Co-ND@DEF nanosystem symbolizes a beacon of hope, guiding the path towards more durable and efficient prostate cancer treatments potentially redefining the therapeutic landscape. By uncovering a new pathway to enhance prostate cancer treatment potential through targeting iron metabolism, our work also paves the road for precision oncology. This may fundamentally alter the paradigm of prostate cancer treatment, providing a more enduring and effective option. Moreover, our nanosystem not only suggests an approach to combat resistant diseases but also directs future research, bringing hope for improved patient outcomes and prostate cancer management. In pursuing these objectives, we aim to substantially improve the quality of life for patients with prostate cancer and make meaningful contributions to men's health worldwide.

Despite its innovative strategy and promising results, several limitations should be acknowledged. Firstly, while the *in vitro* experiments showed significant cytotoxicity against prostate cancer cells, including those resistant to ENZR, the translational potential of this technology remains to be fully validated by extensive *in vivo* studies. Future research should focus on evaluating the long-term efficacy and safety of Pt/Co-ND@DEF in more complex animal models, such as patient-derived xenograft (PDX) models, which better mimic human disease conditions. Secondly, although the study highlighted the synergistic effect of combining Pt/Co-ND@DEF with ENZR, the underlying mechanisms governing this synergy need further exploration, particularly concerning the molecular pathways involved in drug resistance. Addressing these mechanisms could provide insights into developing personalized treatment strategies tailored to individual patients' genetic profiles. Lastly, the manufacturing process of Pt/Co-ND@DEF requires optimization to ensure scalable production and cost-effectiveness essential for clinical translation. In summary, while the current study opens new avenues for prostate cancer treatment, addressing these limitations through comprehensive preclinical validation and mechanistic studies will be crucial for advancing this promising therapeutic modality toward clinical application.

CRedit authorship contribution statement

Mingwei Xu: Conceptualization, Methodology, Investigation, Writing - original draft. **Jun Chen:** Methodology, Investigation, Writing - original draft. **Chengran Huang:** Writing - review & editing, Resources, Funding acquisition. **Cheng Liu:** Conceptualization, Writing - review & editing, Resources, Funding acquisition.

Declaration of competing interest

The authors declare that they have no known competing financial interests or personal relationships that could have appeared to influence the work reported in this paper.

Declaration of Generative AI and AI-assisted technologies in the writing process

The authors confirm that there was no use of artificial intelligence (AI)-assisted technology for assisting in the writing or editing of the manuscript and no images were manipulated using AI.

Acknowledgment

The research/study was approved by the Institutional Review Board at Animal Care and Use Committee of Hubei University of Arts and Science, number HBWL 20240104A, dated 2024.01.07.

References

- Sung, H., Ferlay, J., Siegel, R.L., Laversanne, M., Soerjomataram, I., Jemal, A., Bray, F., 2021. Global cancer statistics 2020: GLOBOCAN estimates of incidence and mortality worldwide for 36 cancers in 185 countries. *CA: A Cancer Journal for Clinicians*, **71**, 209-249. <https://doi.org/10.3322/caac.21660>
- Wang, G., Mao, X., Wang, W., Wang, X., Li, S., Wang, Z., 2024. Bioprinted research models of urological malignancy. *Exploration*, **4**, 20230126. <https://doi.org/10.1002/exp.20230126>
- Higano, C.S., and Crawford, E.D., 2011. New and emerging agents for the treatment of castration-resistant prostate cancer. *Urologic Oncology-Seminars and Original Investigations*, **29**, S1-8. <https://doi.org/10.1016/j.urolonc.2011.08.013>
- Shafi, A.A., Yen, A.E., Weigel, N.L., 2013. Androgen receptors in hormone-dependent and castration-resistant prostate cancer. *Pharmacology & Therapeutics*, **140**, 223-238. <https://doi.org/10.1016/j.pharmthera.2013.07.003>
- Dehkordi, P.R., Mohammadgholi, A., Moghaddam, N.A., 2025. Anticancer activity of synthesized Ag-doped CuO nanoparticles using Ephedra intermedia plant against PC-3 prostate cancer cell line. *Nanomedicine Journal*, **12**, 85-98. <https://doi.org/10.22038/nmj.2024.77128.1877>
- Liang, H., Zhou, B., Li, P., Zhang, X., Zhang, S., Zhang, Y., Yao, S., Qu, S., Chen, J., 2025. Stemness regulation in prostate cancer : Prostate cancer stem cells and targeted therapy. *Annals of Medicine*, **57**, 2442067. <https://doi.org/10.1080/07853890.2024.2442067>
- Scher, H.I., Fizazi, K., Saad, F., Taplin, M.-E., Sternberg, C.N., Miller, K., de Wit, R., Mulders, P., Chi, K.N., Shore, N.D., Armstrong, A.J., Flaig, T.W., Fléchon, A., Mainwaring, P., Fleming, M., Hainsworth, J.D., Hirmand, M., Selby, B., Seely, L., de Bono, J.S., 2012. Increased survival with enzalutamide in prostate cancer after chemotherapy. *New England Journal of Medicine*, **367**, 1187-1197. <https://doi.org/10.1056/nejmoa1207506>
- Virgo, K.S., Rumble, R.B., Talcott, J., 2023. Initial management of noncastrate advanced, recurrent, or metastatic prostate cancer: ASCO guideline update. *Journal of Clinical Oncology*, **41**, 3652-6. <https://doi.org/10.1200/jco.23.00155>
- Liu, Y., Chen, G., You, X., Wang, X., 2024. Cuproptosis Nanomedicine: Clinical challenges and opportunities for anti-tumor therapy. *Chemical Engineering Journal*, **495**, 153373. <https://doi.org/10.1016/j.cej.2024.153373>
- Cheng, B., Li, L., Wu, Y., Luo, T., Tang, C., Zhou, Q., Wu, J., Lai, Y., Zhu, D., Du, T., Huang, H., 2023. The key cellular senescence related molecule RRM2 regulates prostate cancer progression and resistance to docetaxel treatment. *Cell & Bioscience*, **13**, 211. <https://doi.org/10.1186/s13578-023-01157-6>
- Mazzu, Y.Z., Armenia, J., Chakraborty, G., Yoshikawa, Y., Coggins, S.A., Nandakumar, S., Gerke, T.A., Pomerantz, M.M., Qiu, X., Zhao, H., Atiq, M., Khan, N., Komura, K., Lee, G.M., Fine, S.W., Bell, C., O'Connor, E., Long, H.W., Freedman, M.L., Kim, B., Kantoff, P.W., 2019. A novel mechanism driving poor-prognosis prostate cancer: Overexpression of the DNA repair gene, ribonucleotide reductase small subunit M2 (RRM2). *Clinical Cancer Research: An Official Journal of the American Association for Cancer Research*, **25**, 4480-4492. <https://doi.org/10.1158/1078-0432.CCR-18-4046>
- Tury, S., Assayag, F., Bonin, F., Chateau-Joubert, S., Servely, J.L., Vacher, S., Becette, V., Caly, M., Rapinat, A., Gentien, D., de la Grange, P., Schnitzler, A., Lallemand, F., Marangoni, E., Bièche, I., Callens, C., 2018. The iron chelator deferasirox synergises with chemotherapy to treat triple-negative breast cancers. *The Journal of Pathology*, **246**, 103-114. <https://doi.org/10.1002/path.5104>
- Liu, Y., Qi, P., Chen, G., Lang, Z., Wang, J., Wang, X., 2024. Nanoreactor based on single-atom nanoenzymes promotes ferroptosis for cancer immunotherapy. *Biomaterials Advances*, **157**, 213758. <https://doi.org/10.1016/j.bioadv.2024.213758>
- Yuan, Y., Yang, J., Zhuge, A., Li, L., Ni, S., 2022. Gut microbiota modulates osteoclast glutathione synthesis and mitochondrial biogenesis in mice subjected to ovariectomy. *Cell Proliferation*, **55**. <https://doi.org/10.1111/cpr.13194>
- Chen, L., Chen, G., Hu, K., Chen, L., Zeng, Z., Li, B., Jiang, G., Liu, Y., 2023. Combined photothermal and photodynamic therapy enhances ferroptosis to prevent cancer recurrence after surgery using nanoparticle-hydrogel composite. *Chemical Engineering Journal*, **468**, 143685. <https://doi.org/10.1016/j.cej.2023.143685>
- Zhang, Y., Yang, H., Wei, D., Zhang, X., Wang, J., Wu, X., Chang, J., 2021. Mitochondria-targeted nanoparticles in treatment of neurodegenerative diseases. *Exploration*, **1**, 20210115. <https://doi.org/10.1002/exp.20210115>
- Shang, J., Li, H., Wu, B., Jiang, N., Wang, B., Wang, D., Zhong, J., Chen, Y., Xu, X., Lu, H., 2022. CircHIPK3 prevents chondrocyte apoptosis and cartilage degradation by sponging miR-30a-3p and promoting PON2. *Cell Proliferation*, **55**, e13285. <https://doi.org/10.1111/cpr.13285>
- Akerblom, L., Ehrenberg, A., Gräslund, A., Lankinen, H., Reichard, P., Thelander, L., 1981. Overproduction of the free radical of ribonucleotide reductase in hydroxyurea-resistant mouse fibroblast 3T6 cells. *Proceedings of the National Academy of Sciences of the United States of America*, **78**, 2159-2163. <https://doi.org/10.1073/pnas.78.4.2159>
- Chung, M.-H., Aimaier, R., Yu, Q., Li, H., Li, Y., Wei, C., Gu, Y., Wang, W., Guo, Z., Long, M., Li, Q., Wang, Z., 2023. RRM2 as a novel prognostic and therapeutic target of NF1-associated MPNST. *Cellular Oncology*, **46**, 1399-1413. <https://doi.org/10.1007/s13402-023-00819-4>
- Jiang, X., Li, Y., Zhang, N., Gao, Y., Han, L., Li, S., Li, J., Liu, X., Gong, Y., Xie, C., 2022. Correction: RRM2 silencing suppresses malignant phenotype and enhances radiosensitivity via activating cGAS/STING signaling pathway in lung adenocarcinoma. *Cell Bioscience*, **12**, 149. <https://doi.org/10.1186/s13578-022-00882-8>. Erratum for: *Cell Bioscience*, 2021, **11**, 74. <https://doi.org/10.1186/s13578-021-00586-5>
- Liu, C., Yang, J.C., Armstrong, C.M., Lou, W., Liu, L., Qiu, X., Zou, B., Lombard, A.P., D'Abronzo, L.S., Evans, C.P., Gao, A.C., 2019. AKR1C3 promotes AR-V7 protein stabilization and confers resistance to AR-targeted therapies in advanced prostate cancer. *Molecular Cancer Therapeutics*, **18**, 1875-1886. <https://doi.org/10.1158/1535-7163.mct-18-1322>
- Li, Y., Lin, J., He, Y., Wang, K., Huang, C., Zhang, R., Liu, X., 2024. Tumour-microenvironment-responsive Na₂S₂O₈ nanocrystals encapsulated in hollow organosilica-metal-phenolic networks for cycling persistent tumour-dynamic therapy. *Exploration*, **4**, 20230054. <https://doi.org/10.1002/exp.20230054>
- Liu, Y., Ding, L., Chen, G., Wang, P., Wang, X., 2024. A thermo-sensitive hydrogel with prominent hemostatic effect prevents tumor recurrence via anti-anoikis-resistance. *Journal of Nanobiotechnology*, **22**. <https://doi.org/10.1186/s12951-024-02739-3>
- Shao, J., Liu, X., Zhu, L., Yen, Y., 2013. Targeting ribonucleotide reductase for cancer therapy. *Expert Opinion on Therapeutic Targets*, **17**, 1423-1437. <https://doi.org/10.1007/s00280-017-3418-2>
- Rajabpour, A., Afsar, A., Mahmoodzadeh, H., Radfar, J.E., Rajaei, F., Teimoori-Toolabi, L., 2017. MiR-608 regulating the expression of ribonucleotide reductase M1 and cytidine deaminase is repressed through induced gemcitabine chemoresistance in pancreatic cancer cells. *Cancer Chemotherapy and Pharmacology*, **80**, 765-775. <https://doi.org/10.1007/s00280-017-3418-2>